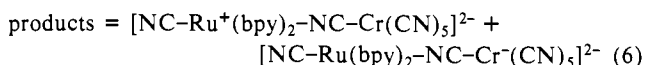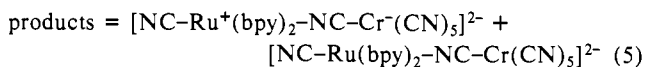the bimolecular annihilation must be of the electron-transfer type, leading to reduction of one of the initially excited chromium centers and to oxidation of a ruthenium center (e.g., eq 5 or 6). Whether the oxidized and reduced centers lie on the same (eq 5)

products = $[NC-Ru^+(bpy)_2-NC-Cr^-(CN)_5]^{2-}$ +
$$[NC-Ru(bpy)_2-NC-Cr(CN)_5]^{2-} \quad (5)$$

products = $[NC-Ru^+(bpy)_2-NC-Cr(CN)_5]^{2-}$ +
$$[NC-Ru(bpy)_2-NC-Cr^-(CN)_5]^{2-} \quad (6)$$

or on different (eq 6) molecules, it is difficult to tell on experimental grounds. It should be noticed that the annihilation

(64) A reviewer has made the interesting suggestion that local dipole-dipole interactions between polynuclear complex ions may occur, and that this may differentiate the behavior of these complexes in the annihilation process from that of $Cr(CN)_6^{3-}$. We tend to maintain, however, the idea that the presence of Ru(II) is *chemically* important, as it seems unlikely that at high ionic strength dipolar interactions alone can make the sharp difference between $Cr(CN)_6^{3-}$ and its bi- and trinuclear derivatives. These interactions could be important at a quantitative level, however, as they may contribute to the stability of the encounter pairs and thus to relatively high values observed for the bimolecular rate constants.

mechanism emerging from this analysis is the bimolecular counterpart of the intramolecular annihilation process envisioned following two-photon excitation of $[(CN)_5Cr-CN-Ru(bpy)_2-NC-Cr(CN)_5]^{4-}$.

Conclusion

The Ru(II)–Cr(III) bimetallic complexes synthesized and studied in this work provide clear-cut examples for the occurrence of intramolecular exchange energy transfer processes. These systems also constitute examples of how covalent coupling to a photosensitizer (chromophore) can improve in several ways (antenna effect, spectral sensitization, reduction of energy losses, protection against photoreactivity) the performance of a light emitter (luminophore). The behavior of the chromium-localized excited state of these Ru(II)–Cr(III) systems is peculiar in several respects, when compared with that of the isolated Cr(III) luminophore. The presence of intervalence-transfer transitions in the ESA and the occurrence of electron-transfer doublet–doublet annihilation are different but interlocked aspects of this peculiarity.

Spectroscopic Studies of the Charge Transfer and Vibrational Features of Binuclear Copper(II) Azide Complexes: Comparison to the Coupled Binuclear Copper Active Site in Met Azide Hemocyanin and Tyrosinase

James E. Pate,[†] Paul K. Ross,[†] Thomas J. Thamann,[†] Christopher A. Reed,[‡] Kenneth D. Karlin,[§] Thomas N. Sorrell,[⊥] and Edward I. Solomon*,[†]

Contribution from the Departments of Chemistry, Stanford University, Stanford, California 94305, University of Southern California, Los Angeles, California 90089, State University of New York (SUNY) at Albany, Albany, New York 12222, and University of North Carolina at Chapel Hill, Chapel Hill, North Carolina 27514. Received October 5, 1988

Abstract: Spectroscopic studies have been performed on a series of copper(II) azide compounds to determine the effects of ligand bridging on their charge-transfer bands. Structurally characterized copper(II) azide model complexes in three limiting geometries (terminal, μ-1,3, and μ-1,1) have been examined using absorption, resonance Raman, and infrared spectroscopies to identify the spectral features of the bound azide. The charge-transfer spectrum of azide bound in a terminal geometry consists of a single intense Π^{nb}_σ band (ϵ = 2000 M^{-1} cm^{-1}) at approximately 400 nm. This feature splits into two bands at 365 (ϵ = 2100 M^{-1} cm^{-1}) and 420 nm (ϵ = 1000 M^{-1} cm^{-1}) in the μ-1,3 dimer. The effects of bridging on the azide-to-copper(II) charge-transfer spectra have been interpreted by using a transition dipole vector coupling model which has been evaluated experimentally with use of structurally defined complexes. The asymmetric intraazide stretch is observed to undergo resonance enhancement in each of the three azide geometries. The Raman excitation profiles have been interpreted by using A-term and B-term formalisms for the μ-1,1 and μ-1,3 complexes, respectively. Mixed isotope ($^{14}N^{14}N^{15}N$) data of the asymmetric intraazide stretch have also been obtained for this series of complexes, and the mixed isotope splitting is found to correlate with the coordination geometry of the azide. A normal coordinate analysis of this data has provided further insight into the origin of the observed mixed isotope splitting and has been used to determine electronic polarization within the azide. These results have been used to further interpret the spectroscopic data from met azide derivatives of mollusc (Busycon) and arthropod (Limulus) hemocyanins and tyrosinase to probe for variations in the active structure among these coupled binuclear copper proteins.

The properties of the coupled binuclear copper active site in hemocyanin, tyrosinase, and the multicopper oxidases have been studied in some detail.[1] In all of these metalloproteins, the active site is involved in interaction with dioxygen. Both hemocyanin and tyrosinase, when in the deoxy [Cu^{I}Cu^I] form, react with dioxygen to produce stable oxygenated species which exhibit similar spectroscopic features. Resonance Raman spectroscopy

has demonstrated that in both systems, the bound dioxygen has been formally reduced to peroxide with an intraligand stretching frequency of ~750 cm^{-1}.[1,2] X-ray absorption edge studies[3] have

[†] Stanford University.
[‡] University of Southern California.
[§] State University of New York (SUNY) at Albany.
[⊥] University of North Carolina at Chapel Hill.

(1) (a) Solomon, E. I. In *Metal Clusters in Proteins*; Que, L., Jr., Ed.; ACS Symposium Series No. 372; American Chemical Society: Washington, DC, 1988; pp 116–150. (b) Solomon, E. I. In *Oxidases and Related Redox Systems*; A. Liss: New York, 1988; pp 309–329. (c) Solomon, E. I.; Pate, J. E.; Westmoreland, T. D.; Kau, L. S.; Allendorf, M. D.; Spira-Solomon, D. J. *Organic and Inorganic Low-Dimensional Crystalline Materials*; Delhaes, P., Drillon, M., Eds.; Plenum Publishing Corp.: 1987; pp 243–269. (d) Solomon, E. I. *Pure Appl. Chem.* **1983**, *55*, 1069–1088. (e) Solomon, E. I.; Penfield, K. W.; Wilcox, D. E. *Structure Bonding* **1983**, *53*, 1–57.

Spectroscopic Studies of Cu(II) Azide Complexes
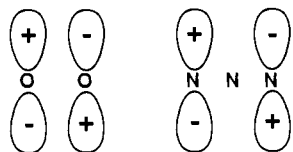
J. Am. Chem. Soc., Vol. 111, No. 14, 1989 5199

Figure 1. Highest occupied valence molecular orbitals of peroxide and azide. (Only in-plane orbitals are drawn.)

indicated that both coppers in the active site are d^9 copper(II). When the peroxide is displaced from oxyhemocyanin, a met derivative [$Cu^{II}Cu^{II}$] is obtained. Both the oxygenated protein and met derivative are EPR nondetectable due to antiferromagnetic coupling between the two copper(II)s. This has been confirmed by SQUID magnetic susceptibility studies[4] that have established a lower limit of $-2J > 600$ cm^{-1} for oxyhemocyanin and $-2J > 400$ cm^{-1} for met hemocyanin ($H_{ex} = -2JS_1 \cdot S_2$). The large antiferromagnetic coupling present in the met and oxy forms[5] requires the presence of a superexchange pathway and, thus, a bridging ligand which cannot be peroxide in the met hemocyanin.

The optical spectroscopic features of oxyhemocyanin are also quite different from those of normal tetragonal copper(II) complexes. Oxyhemocyanin exhibits two intense absorption bands at 345 ($\epsilon = 20\,000$ M^{-1} cm^{-1}) and 580 nm ($\epsilon = 1000$ M^{-1} cm^{-1}) with an additional feature in the circular dichroism near 480 nm ($\Delta\epsilon \sim 1$ M^{-1} cm^{-1}).[6] However, the met aquo derivative possesses a relatively featureless absorption spectrum, except for several weak d-d transitions at 690 nm ($\epsilon = 200$ M^{-1} cm^{-1}). A spectral comparison of the oxy and met derivatives indicates that the intense absorbance features in oxyhemocyanin at 345 and 580 nm and the CD feature at 480 nm are peroxide-to-copper(II) charge-transfer transitions.

When peroxide binds to a single copper(II), two ligand-to-metal charge-transfer transitions are possible from the highest energy occupied Π^* orbitals, one of σ and one of Π symmetry with respect to the peroxo–copper bond.[7,8] The fact that three charge-transfer transitions are observed in oxyhemocyanin indicates the peroxide is interacting with both coppers and leads to further consideration of the charge-transfer transitions of a bridging peroxide.

A transition dipole vector coupling model (TDVC) has been developed to assign the spectral features of the bridging peroxide as well as to predict the relative intensities and energy splittings of the charge-transfer bands.[6] From group theory, a single charge-transfer transition in a monomer (Π^*_σ or Π^*_v) should split into two transitions in the dimer. Consequently, four charge-transfer bands are expected for a bridging peroxide. Application of the TDVC model to the oxyhemocyanin charge-transfer spectrum has indicated that the peroxide binds in a symmetric μ-1,2 geometry. This assignment is consistent with $^{16}O^{18}O$ resonance Raman results[9] as well as with normal coordinate calculations[8] in which the oxyhemocyanin intraperoxide stretching frequency at 728 cm^{-1} did not exhibit a measurable mixed isotope splitting.

Since structural information is not available for oxyhemocyanin,[10,11] the dependence of the charge-transfer spectrum on the ligand binding geometry (terminal vs bridging) has not been tested experimentally. However a met azide derivative of hemocyanin has been prepared in which azide bound to the active site results in several low-energy azide-to-copper(II) charge-transfer transitions.[12] Since the highest occupied orbitals of azide are a set of filled degenerate nonbonding Π orbitals[13] analogous to the set of degenerate Π^* in peroxide[14] (see Figure 1), azide is a spectroscopic analogue for peroxide. Attempts to model the spectroscopic features of met azide hemocyanin have resulted in a series of stable, structurally characterized copper(II) azide model complexes in which a single azide is bound in a terminal,[15,16] μ-1,3,[17,18] or μ-1,1[19-21] geometry. In addition, azide derivatives have been prepared for the binuclear copper(II) active sites in met mollusc and arthropod hemocyanin[12] and met tyrosinase.[22] All of these proteins show azide to copper(II) charge-transfer features in the near ultraviolet; however, significant spectroscopic differences are evident between the different proteins.

In met azide hemocyanin, the azide binding geometry has been interpreted as being a bridging μ-1,3 structure.[23] This was based on the presence of three observed azide-to-copper(II) charge-transfer transitions in (1) the absorbance [380 nm, $\epsilon \sim 2000$ M^{-1} cm^{-1} and 455 nm, $\epsilon = 900$ M^{-1} cm^{-1}], (2) the circular dichroism [a negative feature at 450 nm, $\Delta\epsilon = 1$ M^{-1} cm^{-1}], and (3) the resonance Raman excitation profile of the copper–azide stretch peaking at ~500 nm. Analogous to the TDVC analysis of the peroxide charge-transfer spectrum in oxyhemocyanin, the existence of more than two azide-to-copper(II) charge-transfer bands indicated that the exogenous ligand must bridge. EXAFS in met azide hemocyanin[24] clearly showed a copper–copper outer shell peak, indicating a 3.66 Å copper–copper distance. The only bridging mode consistent with this distance is a μ-1,3 structure.[17-21] The resonance Raman spectrum of the met azide hemocyanin consists of the asymmetric intraazide stretch at 2042 cm^{-1} and

(2) (a) Freedman, T. B.; Loehr, J. S.; Loehr, T. M. J. Am. Chem. Soc. 1976, 98, 2809–2815. (b) Larrabee, J. A.; Spiro, T. G. J. Am. Chem. Soc. 1980, 102, 4217–4223.

(3) (a) Brown, J. M.; Powers, L.; Kincaid, B.; Larrabee, J. A.; Spiro, T. G. J. Am. Chem. Soc. 1980, 102, 4210–4216. (b) Co, M. S.; Hodgson, K. O. J. Am. Chem. Soc. 1981, 103, 2094–2098. (c) Kau, L. S.; Spira, D. J.; Penner-Hahn, J. E.; Hodgson, K. O.; Solomon, E. I. J. Am. Chem. Soc. 1987, 109, 6433–6442.

(4) (a) Solomon, E. I.; Dooley, D. M.; Wang, R. H.; Gray, H. B.; Cerdonio, M.; Mogno, F.; Romani, G. L. J. Am. Chem. Soc. 1976, 98, 1029–1031. (b) Dooley, D. M.; Scott, R. A.; Ellinghaus, J.; Solomon, E. I.; Gray, H. B. Proc. Natl. Acad. Sci. U.S.A. 1978, 75, 3019–3022.

(5) Wilcox, D. E.; Long, J. R.; Solomon, E. I. J. Am. Chem. Soc. 1984, 106, 2186–2194.

(6) Eickman, N. C.; Himmelwright, R. S.; Solomon, E. I. Proc. Natl. Acad. Sci. U.S.A. 1979, 76, 2094–2098.

(7) Karlin, K. D.; Cruse, R. W.; Gultneh, Y.; Hayes, J. C.; Zubieta, J. J. Am. Chem. Soc. 1984, 106, 3372–3374.

(8) Pate, J. E.; Cruse, R. W.; Karlin, K. D.; Solomon, E. I. J. Am. Chem. Soc. 1987, 109, 2624–2630.

(9) Thamann, T. J.; Loehr, J. S.; Loehr, T. M. J. Am. Chem. Soc. 1977, 99, 4187–4189.

(10) The crystal structure of the deoxy Hc has been reported to 3.2 Å resolution: (a) Kuiper, K. A.; Gaastra, W.; Beintema, J. J.; van Bruggen, E. F. J.; Schepman, A. M. H.; Drenth, J. J. Mol. Biol. 1975, 99, 619–629. (b) Gaykema, W. P. J.; Hol, W. G. J.; Vereijen, J. M.; Soeter, N. M.; Bak, H. J.; Beintema, J. J. Nature 1984, 309, 23–29. (c) van Schaick, E. J. M.; Schutter, W. G.; Gaykema, W. P. J.; Schepman, A. M. H.; Hol, W. G. J. J. Mol. Biol. 1982, 158, 457–485. (d) Gaykema, W. P. J.; Volbeda, A.; Hol, W. G. J. J. Mol. Biol. 1985, 187, 255–275.

(11) Structural data on oxy Hc should be available in the not too distant future. (a) Magnus, K. A.; Love, W. E. J. Mol. Biol. 1977, 116, 171–173. (b) Magnus, K. A., personal communication.

(12) Himmelwright, R. S.; Eickman, N. C.; LuBien, C. D.; Solomon, E. I. J. Am. Chem. Soc. 1980, 102, 5378–5388.

(13) (a) Closson, W. D.; Gray, H. B. J. Am. Chem. Soc. 1963, 85, 290–294. (b) McDonald, J. R.; Rabalais, J. W.; McGlynn, S. P. J. Chem. Phys. 1970, 52, 1332–1340.

(14) (a) Kaldor, U.; Shavitt, I. J. Chem. Phys. 1966, 44, 1823–1829. (b) Fink, W. H.; Allen, L. C. J. Chem. Phys. 1967, 46, 2261–2275. (c) Fink, W. H.; Allen, L. C. J. Chem. Phys. 1967, 46, 2276–2284. (d) Gimarc, B. M. J. Am. Chem. Soc. 1970, 92, 266–75.

(15) Ziolo, R. F.; Allen, M.; Titus, D. D.; Gray, H. B.; Dori, Z. Inorg. Chem. 1972, 11, 3044–3050.

(16) (a) Karlin, K. D.; Cohen, B. I.; Hayes, J. C.; Farooq, A.; Zubieta, J. Inorg. Chem. 1987, 26, 147–153. (b) Karlin, K. D., unpublished results.

(17) (a) McKee, V.; Dagdigian, J. V.; Bau, R.; Reed, C. A. J. Am. Chem. Soc. 1981, 103, 7000–7001. (b) McKee, V.; Zvagulis, M.; Dagdigian, J. V.; Patch, M. G.; Reed, C. A. J. Am. Chem. Soc. 1984, 106, 4765–4772.

(18) Sorrell, T. N.; O'Connor, C. J.; Anderson, O. P.; Reibenspies, J. H. J. Am. Chem. Soc. 1985, 107, 4199–4206.

(19) (a) Karlin, K. D.; Hayes, J. C.; Hutchinson, J. P.; Zubieta, J. J. Chem. Soc., Chem. Commun. 1983, 376–378. (b) Karlin, K. D.; Farooq, A.; Hayes, J. C.; Cohen, B. I.; Rowe, T. M.; Sinn, E.; Zubieta, J. Inorg. Chem. 1987, 26, 1271–1280.

(20) Sorrell, T. N. In Biological & Inorganic Copper Chemistry; Karlin, K. D., Zubieta, J., Ed.; Adenine Press: Guilderland, NY, 1986; Vol. II, pp 41–55.

(21) Kahn, O.; Sikorav, S.; Gouteron, J.; Jeannin, S.; Jeannin, Y. Inorg. Chem. 1983, 22, 2877–2883.

(22) Himmelwright, R. S.; Eickman, N. C.; LuBien, C. D.; Lerch, K.; Solomon, E. I. J. Am. Chem. Soc. 1980, 102, 7339–7344.

(23) Pate, J. E.; Thamann, T. J.; Solomon, E. I. Spectrochim. Acta 1986, 42A, 313–318.

(24) Woolery, G. L.; Powers, L.; Winkler, M. E.; Solomon, E. I.; Spiro, T. G. J. Am. Chem. Soc. 1984, 106, 86–92.

5200 *J. Am. Chem. Soc., Vol. 111, No. 14, 1989*

Pate et al.

a copper azide stretch at 397 cm^{-1}. When prepared with $^{14}N^{14}N^{15}N$, the 2042-cm^{-1} peak splits into two components at 2023 and 2035 cm^{-1}, and the 397-cm^{-1} feature shifts to 393 cm^{-1}. The large 12-cm^{-1} splitting of the asymmetric intraazide stretch appears to be inconsistent with a symmetric μ-1,3 binding geometry. However, our prior analysis demonstrated that the splitting of the asymmetric intraazide stretch is not caused by a simple mass effect but instead results from an inequivalence of the two N–N bonds. This inequivalence was rationalized by suggesting an additional interaction of the bound μ-1,3 azide with a protein residue in the active site pocket.

In order to obtain further insight into azide binding in met azide hemocyanin and to evaluate the spectroscopic consequences of ligand bridging on the charge-transfer transitions of copper dimers, a series of structurally characterized copper(II) azide model complexes has been examined. In this study, absorption, resonance Raman, and infrared spectroscopies have been used to identify the spectral features of the azide bound to copper(II) in three limiting geometries (terminal, μ-1,3, and μ-1,1). The azide-to-copper(II) charge-transfer bands have been identified through the use of resonance Raman excitation profiles and by a comparison to spectroscopically "innocent" analogues. The effects on the azide charge-transfer features on going from a terminal to a μ-1,3 azide bridging geometry have been determined and used to evaluate the TDVC model. The mixed isotope ($^{14}N^{14}N^{15}N$) effect of the asymmetric intraazide stretch has also been studied for this series of complexes to (1) gain further insight into the origin of the met azide mixed isotope splitting and (2) determine polarization of the intraazide bonding with variation in small molecule coordination mode. Normal coordinate analyses have been used to compare the vibrational results of the μ-1,3 azide model complexes with those of the met azide hemocyanin. Finally, these studies have been extended to the azide-to-copper(II) charge-transfer data of the met azide derivatives of hemocyanin and tyrosinase to probe differences in exogenous ligand binding in these active sites.

Experimental Section

Both azide- and non-azide-containing model complexes were synthesized according to established procedures: $[Cu_2(L\text{-}Et)(N_3)][BF_4]_2$,[17] $[Cu_2(L\text{-}Et)(OAc)][ClO_4]_2$,[17] $[Cu_2(bpeac)(N_3)][ClO_4]_2 \cdot THF$,[18,20] $[Cu_2(bpeac)(AcO)][ClO_4]_2 \cdot THF$,[18,20] $[Cu_2(N_6O)(N_3)][PF_6]_2$,[20] $[Cu_2(N_6\text{-}O)(OH)][BF_4]_2$,[25] $[Cu_2(L\text{-}O\text{-})(N_3)][PF_6]_2$,[16,19] $[Cu_2(L\text{-}O\text{-})(OH)][PF_6]_2$,[26] $[Cu(L'\text{-}O\text{-})(N_3)]$,[16] $[Cu(L'\text{-}O\text{-})(Cl)]$,[16] $[py_2\text{-}Cu(NO_3)(N_3)]$,[16] $[py_2\text{-}Cu(NO_3)_2]$,[16] $[Cu(Et_4dien)(N_3)Br]$,[15] $[Cu(Et_4dien)Br_2]$,[15] $[Cu_2(tmen)_2(N_3)(OH)][ClO_4]_2$,[21] and $[Cu_2(tmen)_2(OH)_2][ClO_4]_2$.[27] The ligands are defined in the associated references, and the above nomenclature is used in the following text.[28]

Hemocyanin (Hc) from *Busycon Canaliculatum* (Marine Biological Laboratories, Wood's Hole, MA) was purified as previously described,[29] yielding a ~0.1 mM, pH 6.3 solution of oxyhemocyanin. The met azide derivative was prepared[5] by dialyzing oxy Hc in acetate buffer (pH 5.0) containing 100-fold excess fluoride ion (F$^-$) at 37 °C for 48 h, producing met-F$^-$ Hc. Excess F$^-$ was subsequently removed by dialysis in pH 6.3 phosphate buffer. Samples for the azide titration, both CD and absorption, were prepared by directly adding appropriate amounts of azide (dissolved in pH 6.3 phosphate). The samples were allowed to equilibrate at 4 °C for approximately 12 h. Finally, the samples were allowed to come to room temperature over a period of a few hours, and the spectra were taken.

Optical absorption spectra were measured with use of 1-cm quartz cells in a Cary 14 or Cary 17 spectrometer. Circular dichroism spectra

Table I. Energies of the Azide-to-Copper(II) Charge-Transfer Bands of Copper Azide Model Complexes

	energy (cm^{-1})			
	$N_3^- \rightarrow$ Cu(II) charge transfer (1)	(ϵ)	d–d (2)	ΔE [(1) – (2)]
Cu^{NNN}				
$[Cu(Et_4dien)(N_3)Br]$	25800	(1700)	16500	9300
$[py_2\text{-}Cu(NO_3)(N_3)]$	25300	(2300)	15800	9500
$[Cu(L'\text{-}O\text{-})(N_3)]$	25300	(1700)	14700	10600
Cu^{NNN}Cu				
$[Cu_2(L\text{-}Et)(N_3)]^{2+}$	27400	(2100)	14400	13000
	23800	(1000)	14400	9400
$[Cu_2(bpeac)(N_3)]^{2+}$	26600	(2300)	14700	11900
	23000	(950)	14700	8300
$\overset{N}{\underset{N}{\overset{N}{Cu}}}$Cu				
$[Cu_2(N_6O)(N_3)]^{2+}$	24200	(1350)	14800	9400
$[Cu_2(L\text{-}O\text{-})(N_3)]^{2+}$	24000	(1200)	15100	8900

were taken with a Jasco J-500C spectropolarimeter equipped with an S20 photomultiplier tube. Calibration of the CD was achieved by the use of camphor sulfonic acid. In both cases, the resulting spectra were digitized and plotted with an HP 7225B digital plotter interfaced to an IBM PC computer. For each of the azide model complexes, absorption spectra of Nujol mulls were compared with the solution data to check for possible solvation effects. For the hemocyanin, the signals due to the met aquo form were subsequently subtracted from the met azide spectrum. Gaussian analyses of the charge-transfer spectra were performed on a Nicolet 1180E computer with Nicolet's Curve Analysis Program (CAP).

Resonance Raman spectra were measured on a Spex 1403 double monochromator by using a cooled RCA C31034 photomultiplier combined with a Spex digital photometer system and Nicolet 1180E computer. Raman sources included a Coherent CR-18UV argon ion, CR-90K krypton ion, and Rhodamine 6G and Stilbene 3 dye lasers. Raman excitation profiles of $[Cu_2(N_6O)(N_3)][PF_6]_2$ and $[Cu_2(L\text{-}O\text{-})(N_3)][PF_6]_2$ were acquired from room temperature acetonitrile solutions (~2–3 mM) run in a spinning cell. The scattered light at 90° to the incident beam was collected and focused on the monochromator slits. Intensities and band positions were calibrated with use of the solvent peaks. The Raman spectra of $[Cu_2(L\text{-}Et)(N_3)][BF_4]_2$ was obtained from a powder sample in which sodium tetraphenylborate was ground and mixed with the sample as an internal calibrant. Raman data for $[Cu(L'\text{-}O\text{-})(N_3)]$ were obtained from a spinning KBr pellet with KClO$_4$ added as an internal standard. The typical laser power was ~50 mW for all of the model complexes.

Infrared spectra were measured on an IBM IR/98-2A FTIR spectrometer with a typical spectral resolution of 2 cm^{-1}. All of the data in Table II were taken of Nujol mulls (using NaCl windows) of the solid material. Infrared data were not obtained for the $[Cu(Et_4dien)(N_3)Br]$ because of contamination due to residual NaN$_3$. Instead, Raman data were obtained from a methanol solution (spinning cell).

The normal coordinate analysis was based on a Wilson FG matrix method[30] utilizing a modified simple valence force field. The calculations were performed on an IBM PC AT computer (640K memory), which used a modified Schachtschneider Fortran program.[31,32]

Results

Terminal Azide Compounds. Three copper azide monomer complexes which consist of a single azide terminally bound to a copper(II) have been synthesized (Table I). Absorption spectra have been obtained for each of these complexes, and each shows an intense band near 400 nm ($\epsilon \sim 2000$ M^{-1} cm^{-1}) (Figure 2, top). With the exception of $[Cu(L'\text{-}O\text{-})(N_3)]$, comparison with

(25) Sorrell, T. N.; Jameson, D. L.; O'Connor, C. J. *Inorg. Chem.* **1984**, *23*, 190–195.

(26) Karlin, K. D.; Hayes, J. C.; Gultneh, Y.; Cruse, R. W.; McKown, J. W.; Hutchinson, J. P.; Zubieta, J. *J. Am. Chem. Soc.* **1984**, *106*, 2121–2128.

(27) (a) Arcus, C.; Fivizzani, K. P.; Pavkovic, S. F. *J. Inorg. Nucl. Chem.* **1977**, *39*, 285–287. (b) Meek, D. W.; Ehrhardt, S. A. *Inorg. Chem.* **1965**, *4*, 584–587.

(28) L-Et = the anion of N,N,N',N'-tetrakis[2-(1-ethylbenzimidazolyl)]-2-hydroxy-1,3-diaminopropane. bpeac = the anion of 2,6-bis{bis[2-(1-pyrazolyl)ethyl]amino}-p-cresol. N_6O = the anion of 2,6-bis{bis[2-(1-pyrazolyl)ethyl]aminomethyl}-p-cresol. L-O- = the anion of 2,6-bis-[N,N-bis(2-pyridylethyl)aminomethyl]phenol. L'-O- = the anion of 2-[N,N-bis(2-pyridylethyl)amino]methylphenol. py2 = bis[2-(2-pyridyl)ethyl]amine. Et$_4$dien = 1,1,7,7-tetraethyldiethylenetriamine. tmen = N,N,N',N'-tetramethylethylenediamine.

(29) Waxman, L. *J. Biol. Chem.* **1975**, *250*, 3796–3806.

(30) (a) McIntosh, D. F.; Michaelian, K. H. *Can. J. Spectrosc.* **1979**, *24*, 1–10. (b) McIntosh, D. F.; Michaelian, K. H. *Can. J. Spectrosc.* **1979**, *24*, 35–40. (c) McIntosh, D. F.; Michaelian, K. H. *Can. J. Spectrosc.* **1979**, *24*, 65–74.

(31) Schachtschneider, J. H. Technical Report No. 57-65, 1966; Shell Development Co., Emeryville, CA.

(32) Fuhres, H.; Kartha, V. B.; Kidd, K. G.; Krueger, P. J.; Mantsch, H. H. Computer Programs for Infrared Spectroscopy, Bulletin No. 15, National Research Council of Canada, 1976.

Spectroscopic Studies of Cu(II) Azide Complexes

*J. Am. Chem. Soc., Vol. 111, No. 14, 1989* 5201

Table II. Vibrational Frequencies, Calculated Force Constants, and Intraazide Bond Lengths of the Asymmetric Intraazide Stretch of Isotopically Labeled Copper Azide Model Complexes

	vibrational frequencies (cm^{-1})				force constants (mdynes/Å)			bond lengths (Å)		
	^{14}N$_3$	^{15,14}N$_3$, ^{14,15}N$_3$		Δ cm^{-1}	k(N1N2)	k(N2N3)	k_{int}(NN)	N1N2	N2N3	ref
$\overset{123}{\underset{Cu}{NNN}}$										
[Cu(Et$_4$dien)N$_3$Br] (R)	2062	2048, 2054		6	11.8	14.0	1.29	1.145	1.144	15
[py$_2$-Cu(NO$_3$)(N$_3$)] (IR)	2041	2025, 2033		8	11.5	14.2	1.49	a	a	16b
[Cu(L'-O-)(N$_3$)] (IR, R)	2039	2022, 2033		11	11.2	14.5	1.56	1.219	1.231	16a
$\overset{123}{\underset{Cu}{NNN}}\underset{}{Cu}$										
[Cu$_2$(L-Et)(N$_3$)]$^{2+}$ (IR, R)	2025	2013, 2013		0	12.6	12.6	1.36	1.15	1.15	17a
[Cu$_2$(bpeac)(N$_3$)]$^{2+}$ (IR)	2038	2026, <2028		<2	12.5	12.8	1.25	1.147	1.205	18
$\overset{\text{N3}}{\underset{Cu}{\overset{\text{N2}}{\overset{\text{N1}}{}}}}\underset{}{Cu}$										
[Cu$_2$(N$_6$O)(N$_3$)]$^{2+}$ (IR, R)	2065	2045, 2062		17	10.2	15.5	1.49	1.212	1.056	20
[Cu$_2$(L-O-)(N$_3$)]$^{2+}$ (IR, R)	2075	2055, 2073		18	10.1	15.7	1.46	1.117	1.150	16a

^{a} Structure not yet available.
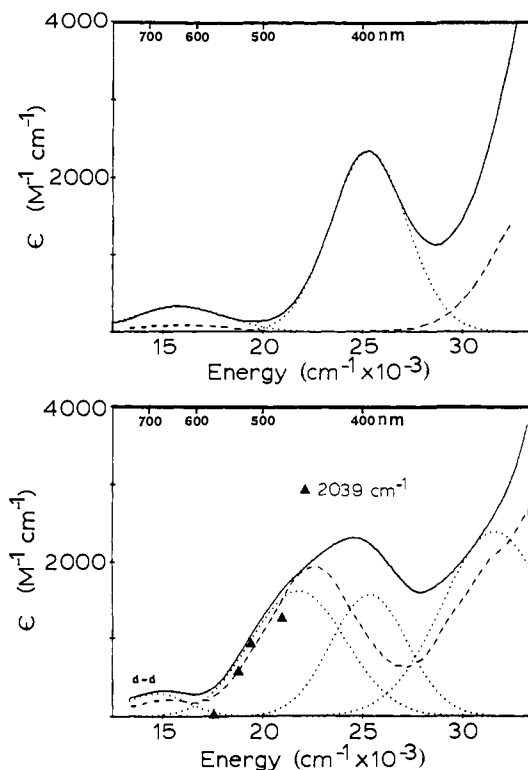
Figure 2. Absorption spectra of acetonitrile solutions of (top) [Py$_2$-Cu-(NO$_3$)(N$_3$)] (—); [Py$_2$-Cu(NO$_3$)$_2$] (- -); and (bottom) [Cu(L'-O-)(N$_3$)] (—); [Cu(L'-O-)(Cl)] (- -). The resonance Raman profile of the 2039-cm^{-1} feature is denoted by (▲). Gaussian components of the azide complexes are indicated by (···).

related non-azide analogues reveals this band to be unique to the azide derivatives.

The optical spectrum of [Cu(L'-O-)(N$_3$)] (Figure 2, bottom) is complicated by spectral contribution from phenolate. The non-azide derivative, [Cu'(L'-O-)(Cl)], has a band at 442 nm (22 600 cm^{-1}, ϵ = 1900 M^{-1} cm^{-1}) which has been assigned as a phenolate to copper(II) charge-transfer transition based on previous resonance Raman results.[33] When azide is substituted for the bound chloride, the observed bandshape changes and appears to shift to higher energy. A Gaussian analysis reveals charge-transfer bands at 395 nm (25 300 cm^{-1}, ϵ = 1700 M^{-1} cm^{-1}), 459 nm (21 800 cm^{-1}, ϵ = 1750 M^{-1} cm^{-1}), and a third Gaussian at 313 nm (32 000 cm^{-1}, ϵ = 2600 M^{-1} cm^{-1}) which is also present
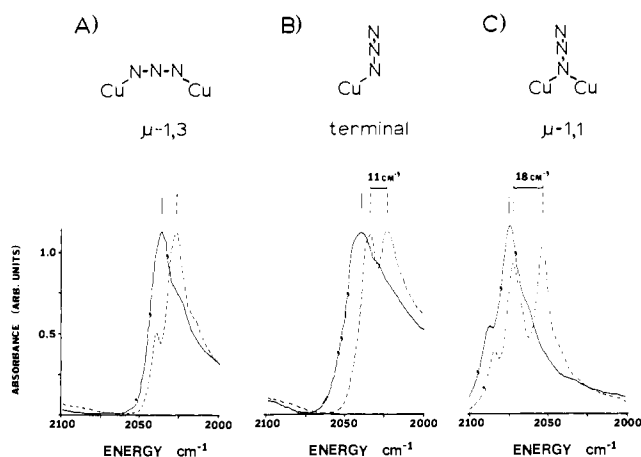
Figure 3. Infrared spectra of Nujol mulls of (a) [Cu$_2$(bpeac)(N$_3$)]-[ClO$_4$]$_2$, (b) [Cu(L'-O-)(N$_3$)], and (c) [Cu$_2$(L-O-)(N$_3$)][PF$_6$]$_2$ prepared with ^{14}N^{14}N^{14}N (—) and ^{14}N^{14}N^{15}N (- -).

in the chloride complex and, therefore, is not an azide-to-copper charger-transfer transition. The Raman data from [Cu-(L'-O-)(N$_3$)] consists of a number of phenolate vibrations[33] in the 1000–1600-cm^{-1} region and an azide mode at 2039 cm^{-1}. The excitation profile of the 2039-cm^{-1} vibration (Figure 2, bottom) shows that the intensity of this mode is enhanced as the laser excitation frequency is increased into the charge-transfer features indicating an azide to copper(II) charge-transfer contribution in this absorption spectral region. Unfortunately, sample degradation prevents the determination of which charge-transfer band is responsible for the observed intensity enhancement. However, the lower energy feature can be assigned as the phenolate-to-copper charge-transfer band based on a comparison with the similar feature in [Cu(L'-O-)(Cl)] and other terminal copper(II) phenolate complexes[34] and the observed Raman enhancement of the phenolate vibrations. Thus, the remaining feature at 395 nm is assigned as an azide-to-copper(II) charge-transfer band. The charge-transfer energies and intensities obtained from Gaussian analyses for the terminal copper azide and the following complexes are included in Table I. To facilitate comparisons between the different complexes, the energies of the charge-transfer transitions have been calibrated relative to the peak energies of the d–d bands of each complex (Table I, ΔE).

Resonance Raman and/or FT-IR data were obtained from each of the terminal mononuclear copper(II) azide model complexes and are summarized in Table II. Excessive fluorescence prevented resonance Raman profiles from being obtained for [Cu-

(33) For a general reference on copper(II) phenolate resonance Raman, see: Pyrz, J. W.; Karlin, K. D.; Sorrell, T. N.; Vogel, G. C.; Que, L., Jr. *Inorg. Chem.* **1984**, *23*, 4581–4584.

(34) Ainscough, E. W.; Bingham, A. G.; Brodie, A. M.; Husbands, J. M.; Plowman, J. E. *J. Chem. Soc., Dalton Trans.* **1981**, 1701–1707.
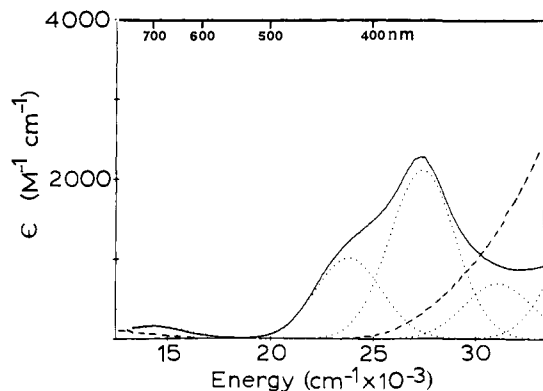
5202 *J. Am. Chem. Soc., Vol. 111, No. 14, 1989*

Pate et al.

Figure 4. Absorption spectra of acetonitrile solutions of $[Cu_2(L-Et)(N_3)][BF_4]_2$ (—) and $[Cu_2(L-Et)(OAc)][ClO_4]_2$ (--). Gaussian components of the azide complex are indicated by (···).

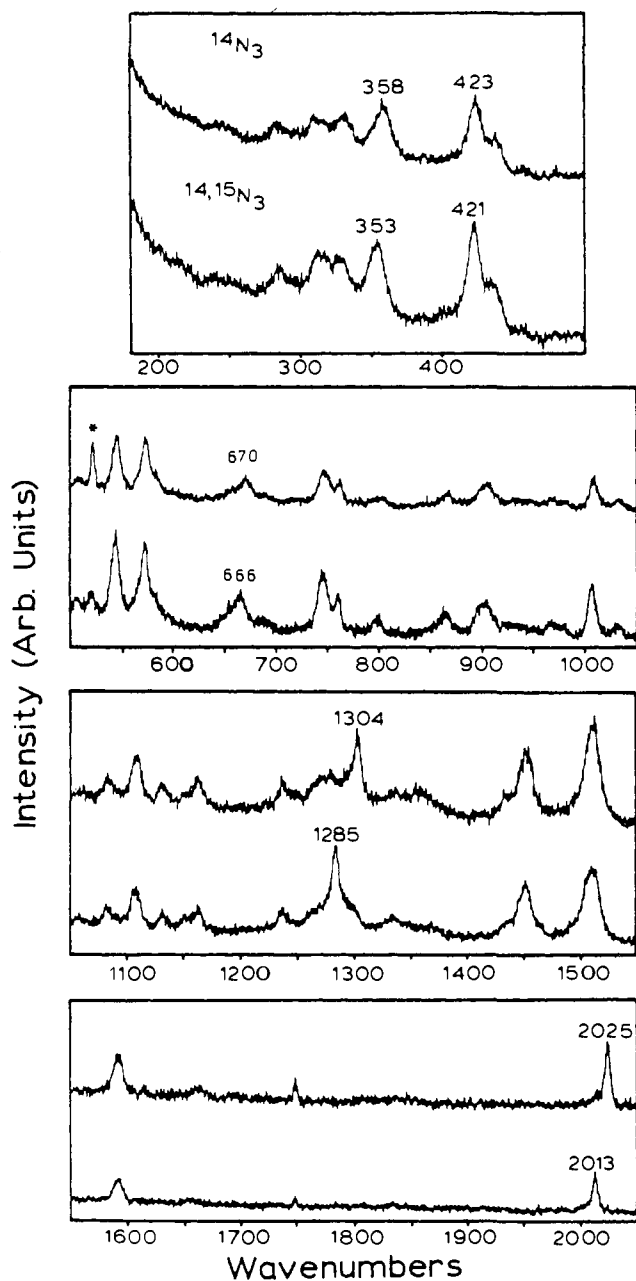**Figure 5.** Resonance Raman spectra of $[Cu_2(L-Et)(N_3)][BF_4]_2$ prepared with $^{14}N^{14}N^{14}N$ (top) and $^{14}N^{14}N^{15}N$ (bottom). Spectral conditions: wavelength, 5309 Å; power at sample, 50 mW; slit width, 4 cm^{-1}; scanning speed, 1 cm^{-1}/s; time constant, 0.5 s; 5 scans. Note: the peak marked with a (*) is due to a plasma line of the laser.

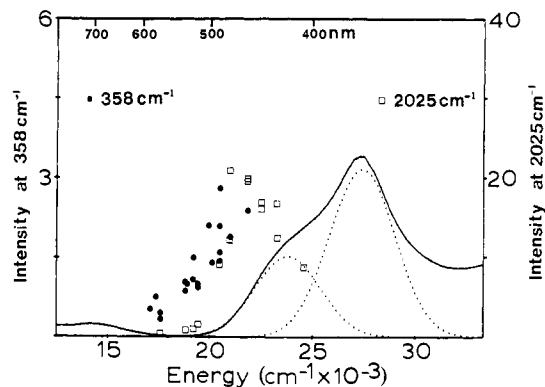**Figure 6.** Resonance Raman profiles of the 358- (●) and 2025-cm^{-1} (□) features of $[Cu_2(L-Et)(N_3)][BF_4]_2$ superimposed on the absorption spectrum and Gaussian resolved azide bands. Note that the scales at left and right give the relative intensities of the asymmetric copper azide and intraazide stretches, respectively.

$(Et_4dien)(N_3)Br]$ and $[py_2-Cu(NO_3)(N_3)]$. However, the vibrational spectra of both complexes exhibit a single band in the 2040–2060-cm^{-1} region which shifts and undergoes a 6–8 cm^{-1} splitting when prepared with $^{14}N^{14}N^{15}N$. In addition, infrared data reveals that the 2039-cm^{-1} band in $[Cu(L'-O-)(N_3)]$ splits into two components at 2022 and 2033 cm^{-1} in the $^{14,15}N_3$ derivative[35] (Figure 3B).

μ-1,3 Azide Compounds. The crystal structures of two different dibridged copper(II) dimers with a single μ-1,3 azide bridge and a second alkoxide or phenolate bridge have been reported[17,18] (Table I). The absorption spectra reveal the presence of an intense charge-transfer band near 375 nm (ϵ = 2300 M^{-1} cm^{-1}) with an associated shoulder at ~440 nm (ϵ ~ 1200 M^{-1} cm^{-1}). A Gaussian analysis resolves these features into two charge-transfer bands at 365 nm (27400 cm^{-1}, ϵ = 2100 M^{-1} cm^{-1}) and 420 nm (23800 cm^{-1}, ϵ = 1000 M^{-1} cm^{-1}) for $[Cu_2(L-Et)(N_3)][BF_4]_2$ (Figure 4). Comparison of the absorption spectrum of the azide complex with its non-azide analogue demonstrates that these bands are associated with the bound azide. Similar bands are observed at 376 nm (26600 cm^{-1}, ϵ = 2300 M^{-1} cm^{-1}) and 434 nm (23000 cm^{-1}, ϵ = 950 M^{-1} cm^{-1}) for $[Cu_2(bpeac)(N_3)][ClO_4]_2$·THF. However, the $[Cu_2(bpeac)(AcO)][ClO_4]_2$·THF also shows a much weaker transition (ϵ = 120 M^{-1} cm^{-1}) in the same spectral region (437 nm, 22900 cm^{-1}),[20] which is likely due to phenolate-to-copper(II) charge-transfer. This feature is probably contributing weakly (ϵ ~ 100–200 M^{-1} cm^{-1}) to the intensity of the observed azide features in the $[Cu_2(bpeac)(N_3)][ClO_4]_2$·THF dimer.

The resonance Raman spectrum of $[Cu_2(L-Et)(N_3)][BF_4]_2$ (Figure 5) has been obtained with both $^{14}N_3$ and labeled azide and shows several features associated with the bound azide. In the metal ligand region, the peaks at 358 and 423 cm^{-1} are lowered to 353 and 421 cm^{-1} with $^{14,15}N_3$. The intraligand region shows three additional peaks at 670, 1304, and 2025 cm^{-1} that shift to 666, 1285, and 2013 cm^{-1}, respectively, upon isotopic substitution. The resonance Raman profile (Figure 6) shows that the intensities of two of these modes are enhanced. The intensity of the 2025-cm^{-1} vibration is maximized at approximately 460–465 nm (21500–21700 cm^{-1}) which is at lower energy than the 420-nm charge-transfer band. Due to low signal intensity, it is unclear as to which transition is causing the intensity enhancement of the 358-cm^{-1} vibration.[36] Resonance Raman data could not be obtained for $[Cu_2(bpeac)(N_3)][ClO_4]_2$·THF due to its lack of stability in the laser beam. However, infrared data (Figure 3A) exhibit an azide vibration at 2038 cm^{-1}. With $^{14,15}N_3$, this band shifts to 2026 cm^{-1} and may broaden slightly (<2–3 cm^{-1}). The crystal structure of $[Cu_2(bpeac)(N_3)][ClO_4]_2$·THF[18] shows that

(35) Mixed and normal isotope data was obtained from the infrared due to the limited amounts of available material and pronounced decomposition in the Raman experiments.

(36) Depolarization ratios were not obtained because of polarization scrambling by the sample particles and the poor quality of solution spectra.

Spectroscopic Studies of Cu(II) Azide Complexes

J. Am. Chem. Soc., Vol. 111, No. 14, 1989 5203
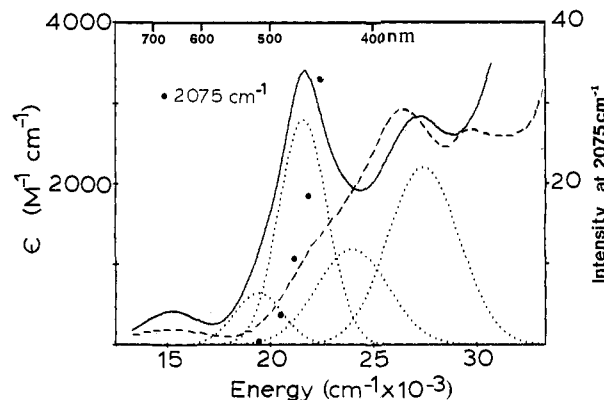
Figure 7. Absorption spectra of an acetonitrile solutions of [Cu$_2$-(L-O-)(N$_3$)][PF$_6$]$_2$ (—) and [Cu$_2$(L-O-)(OH)][PF$_6$]$_2$·THF (--). The resonance Raman profile of the 2075-cm^{-1} feature is denoted by (●). Gaussian components of the azide complex are indicated by (⋯). The scale at right indicates the relative intensity of the asymmetric intraazide stretch.
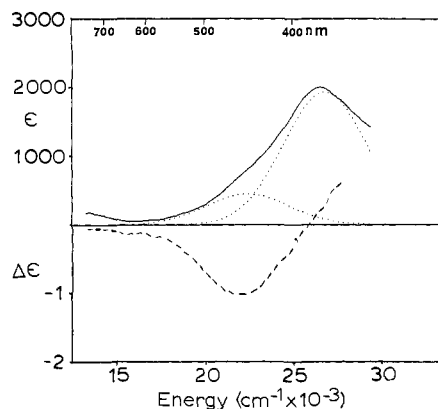

Figure 8. Absorption (—) and circular dichroism (--) difference spectra of met azide hemocyanin (Busycon). Gaussian components are indicated by (⋯).

the N1-N2 bond length in the azide is shorter than that of the N2-N3 (1.14 vs 1,21 Å) which may contribute to the broadening.

μ-1,1 Azide Compounds. Three different dibridged μ-1,1 copper(II) complexes[19-21] exist with a single azide bridge and a second phenolate or hydroxide bridge (Table I). The absorbance spectra of [Cu$_2$(N$_6$O)(N$_3$)][PF$_6$]$_2$ and [Cu$_2$(L-O-)(N$_3$)][PF$_6$]$_2$ exhibit an intense charge-transfer band at 460 nm ($\epsilon \sim$ 3000 M^{-1} cm^{-1}) and other unresolved features at higher energy (Figure 7). Gaussian resolutions of the azide and hydroxide absorption spectra reveal the presence of a band at 460 nm in both complexes. Similar fits of the azide derivatives demonstrate that the large intensity at 460 nm is probably resulting from an increase of an existing charge-transfer feature. ([Cu$_2$(tmen)$_2$(N$_3$)(OH)][ClO$_4$]$_2$ and [Cu$_2$(tmen)$_2$(OH)$_2$][ClO$_4$]$_2$ were also examined but appeared to decompose when dissolved in a variety of solvents.)

The resonance Raman spectra of [Cu$_2$(N$_6$O)(N$_3$)][PF$_6$]$_2$ and [Cu$_2$(L-O-)(N$_3$)][PF$_6$]$_2$ exhibit a single azide related peak at 2065-2075 cm^{-1} which shifts and splits by 18 cm^{-1} in the ^{14}N^{14}N^{15}N derivative (Figure 3C, Table II). The resonance Raman excitation profile (Figure 7) of the asymmetric intraazide stretch of each of these μ-1,1 complexes indicates that the intense 460-nm band is not an azide-to-copper(II) charge-transfer feature, since the profile maximizes to higher energy than the band maximum. Previous resonance Raman work[33] indicates that the 460-nm band is likely due to a phenolate-to-copper(II) charge-transfer transition in both the hydroxide and azide derivatives. Depolarization ratio of this Raman feature is 0.4 for each complex.

Met Azide Hemocyanin. The azide-to-copper(II) charge-transfer absorption and CD spectra of met azide hemocyanin are given in Figure 8. In order to compare this spectrum with those of related complexes, it is necessary to establish that the observed charge-transfer features are associated with a single azide binding
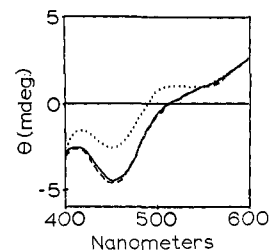
Figure 9. Circular dichroism spectra of 3 mM Hc with (1) [N$_3^-$]$_T$ = 6 mM (—); (2) dialyzed in 4 mM N$_3^-$ (--); and (3) dialyzed in 2 mM N$_3^-$ (⋯). (See text for details of experiment.)

to the active site. Binding constants calculated from direct reciprocal and Scatchard plots[37] of both the absorption and the CD titration data indicate a single binding constant of $\sim$500 M^{-1} (per binuclear site). Since the equilibrium free azide concentration from direct addition to the met hemocyanin is dependent upon the number of azides binding to the active site, it is possible to distinguish between the binding of a single azide vs two azides (with similar binding constants) by comparing the circular dichroism spectra of the following three met azide samples. (1) Azide was directly added to a 3 mM met aquo hemocyanin such that the total azide concentration was 6 mM. On the basis of K_{eq} = 500 M^{-1}, the equilibrium free azide concentration of this sample should be $\sim$4 mM if one azide is binding to the active site or $\sim$2 mM if two azides are binding. (2) An 800-μL sample of met aquo hemocyanin was dialyzed vs a large volume (1 L) of 4 mM azide (dissolved in pH 6.3 phosphate buffer). (3) An 800-μL sample was analogously dialyzed vs a 2 mM azide solution. The CD signals of the three samples are shown in Figure 9, and the signal from the direct addition of azide (sample 1) is seen to directly match that of the 4 mM dialysis, indicating a single azide binding to the active site generates the spectra in Figure 8.
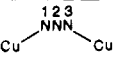
Analysis

Vibrations. A normal coordinate analysis has been used to assign the vibrational features associated with [Cu$_2$(L-Et)(N$_3$)][BF$_4$]$_2$. The asymmetric stretch, symmetric stretch, and the bending modes of the bound azide at 2025 (2013 with ^{14,15}N$_3$), 1304 (1285), and 670 (666) cm^{-1}, respectively, can be assigned by comparison to the spectrum and prior calculations of the free ligand.[38] Two copper azide stretching modes are expected, the asymmetric and symmetric, and two features in the metal ligand region exhibit an appreciable mixed isotope effect when prepared with ^{14}N^{14}N^{15}N; a band at 358 cm^{-1} shifts to 353 cm^{-1}, and a band at 423 cm^{-1} moves to 421 cm^{-1} (Figure 5).

Calculations with a five atom cis μ-1,3 Cu$_2$N$_3$ system indicate that the asymmetric Cu-N$_3$ stretch is at higher energy and shows a larger frequency shift upon isotopic perturbation with ^{14}N^{14}N^{15}N relative to the symmetric mode. An estimate of the range in magnitude of the isotopic shifts for both the asymmetric and symmetric copper azide stretching modes is shown in Figure 10. These results were obtained from a five atom calculation by using the geometric parameters and the intraazide vibrational frequencies for the [Cu$_2$(L-Et)(N$_3$)][BF$_4$]$_2$ complex. A modified simple valence force field, which included a single N-N stretching force constant [k(N-N)], a Cu-N stretching force constant [k-(Cu-N)], an N-N-N bending force constant [δ(N-N-N)], a Cu-N-N bending force constant [δ(Cu-N-N)], and a stretch-stretch interaction force constant [k_{int}(N-N)], was used for each of the calculations in which only planar vibrations were considered. The asymmetric copper azide stretch was fixed at a series of frequencies between 200 and 550 cm^{-1}, and the symmetric copper azide was allowed to vary. From Figure 10, it is seen that the isotopic shift of the asymmetric copper azide stretch varies linearly with the frequency, while the isotopic shift of the symmetric copper azide stretch remains relatively constant (<2 cm^{-1}). On the basis

(37) Marshall, A. In *Biophysical Chemistry: Principles, Techniques, and Applications*; Wiley: New York, 1978; pp 70-85.
(38) Gray, P.; Waddington, T. C. *Trans. Faraday Soc.* **1957**, *53*, 901-908.

5204   *J. Am. Chem. Soc., Vol. 111, No. 14, 1989*

Pate et al.

Table III. Normal Coordinate Calculations of the μ-1,3 Copper Azide Geometry in [Cu(L-Et)(N$_3$)][BF$_4$]$_2$ and Met Azide Hemocyanin

$\overset{1\ 2\ 3}{\underset{Cu}{\diagup}}\overset{NNN}{\diagdown}Cu$	$^{14}N^{14}N^{14}N$ (and $^{14}N^{14}N^{15}N$) azide frequencies (cm^{-1})			
	$v(N_3)_{asym}$	$v(N_3)_{sym}$	$v(N_3)_{bend}$	$v(Cu-N_3)_{asym}$
[Cu$_2$(L-Et)(N$_3$)]$^{2+}$	2025	1304	670	358
	(2013)	(1285)	(666)	(353)
met azide	2042			397
hemocyanin	(2023, 2035)			(393)

	refined force constants (mdynes/Å)					
	k(N1N2)	k(N2N3)	k_{int}(NN)	δ(NNN)	k(CuN)	δ(CuNN)
[Cu$_2$(L-Et)(N$_3$)]$^{2+}$	12.6	12.6	1.36	0.67	0.81	0.15
met azide	11.2	14.5	1.55	0.67	0.96	0.24
hemocyanin						
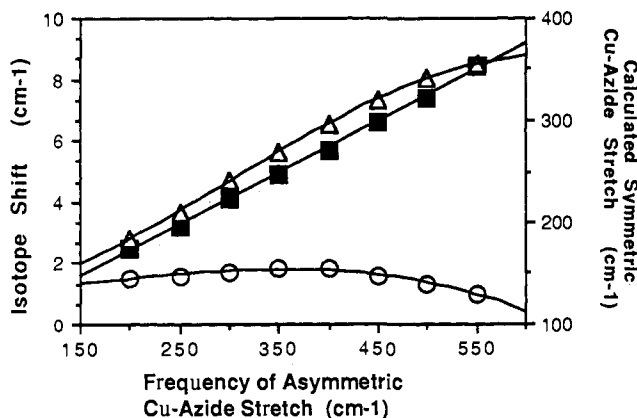
Figure 10. Calculated isotopic shifts of the symmetric (O) and asymmetric (■) copper azide stretching frequencies of a five body cis μ-1,3 copper azide geometry (scale at left). The calculated symmetric stretch of the $^{14}N^{14}N^{14}N$ complex are indicated by (△) (scale at right).

Figure 11. Absorption energy level diagram for a mononuclear copper azide complex.

of its larger isotopic shift, the Raman peak at 358 cm^{-1} must be assigned as the asymmetric copper azide stretch. These normal coordinate calculations thus show that the mode at 423 cm^{-1} cannot be the symmetric copper azide stretch (as it should appear at approximately 270 cm^{-1}) but instead must reflect vibrational coupling of other metal ligand modes with the copper azide vibrations. An examination of the 270-cm^{-1} spectral region reveals candidates for the symmetric copper azide stretch at 283, 309, and 331 cm^{-1}, and a broad feature at centered at $\sim$242 cm^{-1}. Unfortunately, the lack of a resolvable isotopic shift or resonance Raman enhancement precludes a definite assignment.

Analysis of the charge-transfer spectrum of met azide hemocyanin (vide infra) combined with a 3.6 Å copper–copper distance from EXAFS indicates that azide binds in a μ-1,3 geometry, analogous to [Cu$_2$(L-Et)(N$_3$)][BF$_4$]$_2$. The resonance Raman spectrum of met azide hemocyanin shows peaks at 397 and 2042 cm^{-1} which shift to lower frequency upon isotopic substitution with $^{14}N^{14}N^{15}N$, with the 2042-cm^{-1} feature splitting into two components at 2023 and 2035 cm^{-1}.[23] The magnitude of the isotopic shift of the 397-cm^{-1} vibration with $^{14}N^{14}N^{15}N$ indicates that it must also be assigned as the asymmetric copper azide stretch. Thus both the asymmetric copper azide and intraligand stretches are at higher energy in hemocyanin relative to the [Cu$_2$(L-Et)(N$_3$)][BF$_4$]$_2$. However, only hemocyanin shows a splitting of the intraligand mode. Table III presents normal coordinate calculations for both the [Cu$_2$(L-Et)(N$_3$)][BF$_4$]$_2$ and met azide hemocyanin vibrational data which indicate that these differences between the two systems derive from the strengths of the copper–azide bonds (as shown by the copper–azide force constants) and inequivalence within the bound azide in hemocyanin. The copper–azide force constant [k(Cu–N)] increases by 0.15 mdynes/Å in going from the model complex to met azide hemocyanin, which provides an estimate of the increased strength of the copper–azide bond in the protein. As indicated earlier, the inequivalence within the bound azide in met azide Hc is associated with differences in k(N1–N2) and k(N2–N3). These split (11.2 and 14.5 mdyne/Å) about the value (12.6 mdyne/Å) for the symmetric μ-1,3 model.
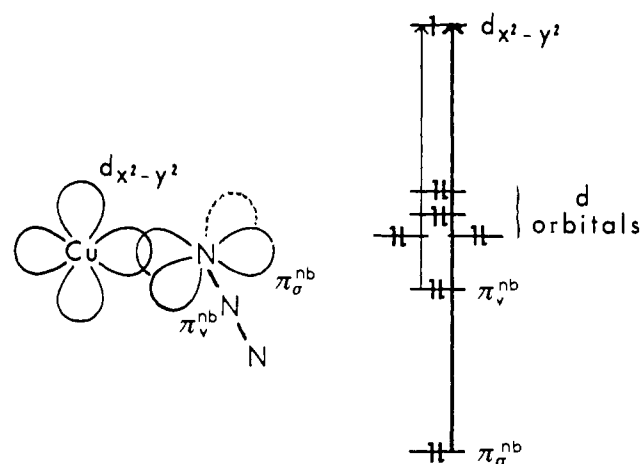
In order to gain further insight into the degree of inequivalence within the azide bond in the three geometries at the top of Figure 3 and in met azide hemocyanin, normal coordinate calculations were done on all the vibrational data of Table II. The calculations assumed a structure consisting of only the copper(s) and the azide and used the geometrical parameters obtained from the appropriate crystal structures. Table II (middle three columns) presents the N–N force constants obtained from a fit to the experimental asymmetric intraazide mixed isotope splittings. These results indicate that the inequivalence exhibited by the met azide hemocyanin is similar to that introduced by binding a copper to one end of a free azide. The crystal structures of the three terminal copper azide complexes indicate that this inequivalence correlates to differences between (N1–N2) and (N2–N3) bonds of less than 0.01 Å.

Charge-Transfer Transitions. The highest energy occupied orbitals of azide are a filled degenerate set of Π nonbonding (Π^{nb}) (Figure 1) which split in energy upon binding to the copper (Figure 11). One Π^{nb} orbital (Π^{nb}_{σ}) forms a σ bond to the d$_{x^2-y^2}$ orbital of the copper and is strongly stabilized by this interaction. The other Π^{nb} orbital (Π^{nb}_v) is perpendicular to the copper d$_{x^2-y^2}$ plane and undergoes a weaker Π bonding interaction. Thus, the Π^{nb}_{σ} to Cu(II) d$_{x^2-y^2}$ transition should be at higher energy relative to that of the Π^{nb}_v. Further, the intensity of the Π^{nb}_{σ} transition should be greater due to its better overlap with the copper d$_{x^2-y^2}$ orbital. An estimate of the $\Pi^{nb}_{\sigma}-\Pi^{nb}_v$ splitting may be obtained from ab initio calculations of HN$_3$, which give a 12 000-cm^{-1} splitting of the Π^{nb} orbitals resulting from a strong σ interaction with the proton.[39] Replacement of the proton with a copper(II) should result in a smaller splitting from both a weaker σ bonding interaction with the copper and an additional Π bonding interaction of the Π^{nb}_v with the d orbitals.

(39) Wyatt, J. F.; Hillier, I. H.; Saunders, V. R.; Connor, J. A.; Barber, M. *J. Chem. Phys.* 1971, 54, 5311–5315.
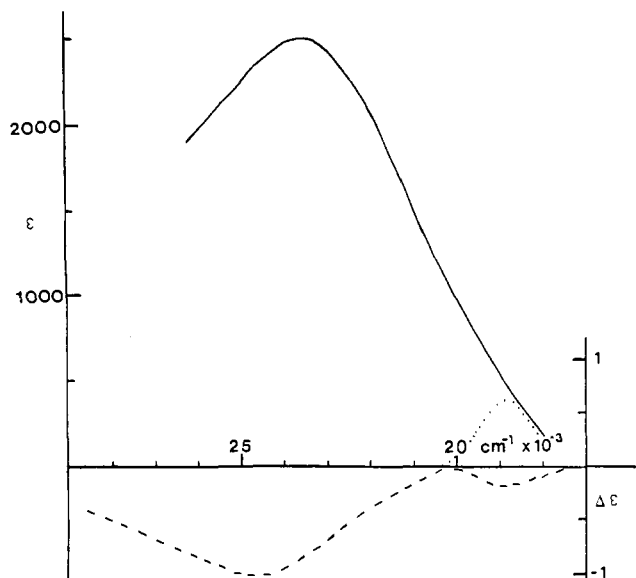
Figure 12. Absorption (—) and circular dichroism (--) of met apo azide hemocyanin. Gaussian components are indicated by (···). (Spectra were recorded at room temperature, adapted from ref 12.)

Table IV. Symmetries and Selection Rules for the Charge Transfer Transitions in a Monomer and C_{2v} Dimer System

|	monomer C_{2v} symmetry	dimer C_{2v} symmetry	polarization
$\Pi^{nb}_v \rightarrow d_{x^2-y^2}$	B_1	A_2	R_z
		B_2	y, R_x
$\Pi^{nb}_\sigma \rightarrow d_{x^2-y^2}$	A_1	A_1	z
		B_1	x, R_y

Although two azide-to-copper(II) charge-transfer transitions are predicted for a terminal copper(II) azide complex, a comparison of the spectroscopic features of these models with those of their non-azide analogues reveals only a single azide-to-copper(II) charge-transfer band at 400 nm. On the basis of its significant intensity ($\epsilon \sim 2000$ M^{-1} cm^{-1}) and the lack of comparable absorbance features within 5000 cm^{-1}, the 400-nm band is assigned as the Π^{nb}_σ-to-copper(II) charge-transfer transition. Support of this assignement comes from the spectrum of met apo azide hemocyanin[12] (Figure 12) which contains a single copper(II) in the hemocyanin active site. The optical activity of the protein ligand allows the azide-to-copper(II) charge-transfer features to contribute to the circular dichroism spectrum (which probes the magnetic dipole character of these transitions). In addition to the absorption peak at 420 nm ($\epsilon \sim 2000$ M^{-1} cm^{-1}) which compares to the peak observed for the model complexes, the CD spectrum exhibits an additional peak at 525 nm. Resolution of the absorption spectrum indicates that the ϵ of this peak cannot be greater than 300 M^{-1} cm^{-1}. The low absorbance intensity derives from poor overlap of the Π^{nb}_v with the copper(II) $d_{x^2-y^2}$ orbital, while the relatively large CD intensity in met apo hemocyanin reflects the fact that there should be significant magnetic dipole character for a Π^{nb}_v to $d_{x^2-y^2}$ transition as this involves rotation of the electron into the $d_{x^2-y^2}$ orbital.

The transition dipole vector coupling model predicts that azide bridging two copper(II)s in either a μ-1,3 or a μ-1,1 geometry should result in four (spin allowed) charge-transfer transitions: the symmetric and antisymmetric combinations of the monomeric Π^{nb}_σ and Π^{nb}_v transitions. Only two features at ~365 nm ($\epsilon \sim 2000$ M^{-1} cm^{-1}) and ~420 nm ($\epsilon \sim 1000$ M^{-1} cm^{-1}) are observed for the μ-1,3 dimer (Figure 4). However, for the terminal copper-azide monomers only the Π^{nb}_σ-to-copper(II) charge-transfer band contributes to the absorbance spectrum with appreciable intensity. As this will split into two transitions in the dimer (Table IV, A_1 and B_1 components), these can be associated with the two observed features in the μ-1,3 dimer. It should be noted that the crystal structure of [Cu$_2$(L-Et)(N$_3$)][BF$_4$]$_2$ indicates that the two

Table V. Charge-Transfer Energy Splittings and Intensity Ratios

		experimental	
$\Pi^{nb}_\sigma \rightarrow d_{x^2-y^2}$	calcd	[Cu$_2$(L-Et)(N$_3$)]$^{2+}$	Met N$_3$ Hc
$\Delta E(A_1 - B_1)$ (cm^{-1})	275	3600	4400
$I(A_1)/I(B_1)$	8.6	2.1	2.1

Scheme I
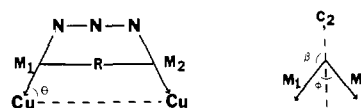
copper atoms are crystallographically equivalent.[17a] Therefore, the two observed azide-to-copper(II) charge-transfer bands must result from interactions between two equivalent transition moments, rather than corresponding to inequivalent transitions to each copper.

The intensity ratios of the A_1 and B_1 components of Π^{nb}_σ can be estimated from the vector sum and difference of the charge-transfer moments to each copper(II), while the energy splittings can be estimated from the Coulomb interactions between these transition moments. These are given by eq 1 and 2 which have been used to calculate the intensity ratios and energy splittings for the μ-1,3 dimer complex (Table V). The parameters are defined in Scheme I: M_1 and M_2 are the transition dipoles on monomers 1 and 2, respectively, separated by a distance R. Θ is the angle between the transition dipole and the copper–copper vector, Φ is the angle between the two transition dipoles, and β is the angle between the dipole and the C_2 axis.

$$\Delta E(A - B) = \frac{-2|M|^2}{R^3} \{3 \cos^2 \Theta - \cos \Phi\} \quad (1)$$

$$\frac{I_A}{I_B} = \frac{|M_1 + M_2|}{|M_1 - M_2|} = \frac{\cos^2 \beta}{\sin^2 \beta} \quad (2)$$

An intensity ratio of 8.6 for the A_1 and B_1 components of Π^{nb}_σ has been calculated using eq 2 and the following structural parameters obtained from [Cu$_2$(L-Et)(N$_3$)][BF$_4$]$_2$: Cu–N$_3$ = 2.04 Å, R = 2.96 Å, Θ = 71.2°, Φ = 37.6°, and β = 18.8°. Since the A_1 component has the dominant intensity, it can be assigned as the feature at 365 nm. The band at 420 nm is similarly assigned as the B_1 component of Π^{nb}_σ. However, it should be noted that the experimental intensity (I_{365}/I_{420} = 2.1) is lower than the calculated value.

The resonance Raman enhancement profile provides insight into the deviation in the experimental intensity ratio of $I(A_1)/I(B_1)$ relative to that expected for coupled transition moments. The intensity of the asymmetric intraazide stretch at 2025 cm^{-1} undergoes the dominant resonance enhancement. As the rigorous site symmetry in the [Cu$_2$(L-Et)(N$_3$)][BF$_4$]$_2$ crystal (space group = $C2/m$) is C_2, this vibration must have B symmetry (B_1 in an effective C_{2v} symmetry). Enhancement of a nontotally symmetric mode derives from a B-term type mechanism, which involves vibronic coupling of a weak transition with a strong absorbance band. Large enhancements of nontotally symmetric vibrations are expected for modes which are particularly effective at mixing electronic transisitions.[40] Calculations of the equilibrium configurations of N$_3^-$ and N$_3$ (radical) indicate that the primary distortion upon removing an electron from the N$_3^-$ is an elongation of one of the nitrogen–nitrogen bonds and a decrease in the other.[41] This distortion parallels that of the asymmetric intraazide normal coordinate and should be effective at vibronic coupling to the intense A_1 component of Π^{nb}_σ. In addition, from group theory only the B_1 excited state can be mixed through a b_1 vibration,

$$\left\langle \Psi(B_1) \left| \frac{\partial V}{\partial Q_{B_1}} \right| \Psi(A_1) \right\rangle \neq 0$$

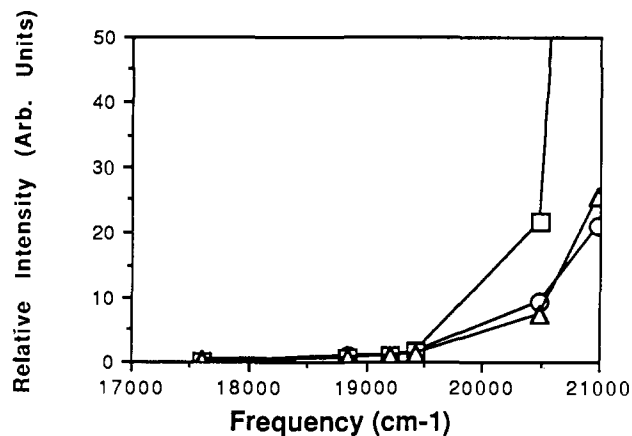thus consistent with the assignment of the 420-nm band as the B_1 component of Π^{nb}_σ.

Figure 13. Calculated resonance Raman A-term ($\square$) and B-term ($\bigcirc$) profiles for the asymmetric intraazide stretch in $[Cu_2(L\text{-Et})(N_3)][BF_4]_2$. The experimental relative intensities are indicated by ($\triangle$).

The larger intensity of the B_1 component (as compared to the TDVC calculation) requires 23% mixing of the A_1 component. Support for both the mixing of the A_1 and B_1 components and the assignment of the B-term enhancement comes from a fit of a B-term profile to the 2025-cm^{-1} data (Figure 13). This was performed by calculating the relative intensities of the 2025-cm^{-1} Raman peak in the preresonance edge of the profile as a function of excitation wavelength using either an Albrecht A or B term[42] and assuming that $v_e = 21\,775$ cm^{-1} (the peak of the experimental profile). For the B-term calculation, the band at 365 nm (27 400 cm^{-1}) was used for v_s.

For B-term profiles, equal intensity maxima in the excitation profiles are expected from both the 0–0 electronic and 0–1 vibronic origins.[40] The experimental observation of the peaking of the 2025-cm^{-1} excitation profile ~ 2000 cm^{-1} below the apparent absorption maximum suggests that it is reflecting a maximum associated mostly with the 0–0 origin of the 420-nm absorption band. Calculations show that this type of inequivalence in the B-term excitation profile intensities can derive from differences in vibronic bandwidths which would reflect the fact that the 0–0 transition is less subject to vibrational relaxation.[43] It should also be noted that the isotope effect of the 358-cm^{-1} mode defines it as the asymmetric copper azide stretch. Therefore, it has B_1 symmetry and must also derive from a B-term vibronic coupling mechanism.

Finally, a comparison of the experimental and TDVC calculated A_1–B_1 energy splittings of 3600 and 275 cm^{-1}, respectively, indicates that the calculated values severely underestimate the total energy splitting. Although, the sign of the energy splitting is correct, the Coulomb coupling of transition moments is clearly not the only contribution to the total energy splitting. Additional exchange contributions will be discussed in detail in the next section.

Similar to the μ-1,3 azide dimers, two (singlet) Π^{nb}_{σ} azide-to-copper(II) charge-transfer bands would also be expected for μ-1,1 azide complexes. Although only two bands at 365 and 460 nm are clearly resolved in the absorption spectra of the μ-1,1 azide complexes (the latter being assigned as a phenolate charge-transfer transition, vide supra), Gaussian fits of $[Cu_2(N_6O)(N_3)][PF_6]_2$ and $[Cu_2(L\text{-O-})(N_3)][PF_6]_2$ (Figure 7) indicate the possibility of an additional absorption band at 420 nm ($\epsilon = 1000$ M^{-1} cm^{-1}). Calculated profiles of the preresonance A-term enhancement of the asymmetric intraazide stretch (Figure 14) indicate that the observed enhancement results from the absorbance band at ~ 420 nm, rather than from the higher energy feature at 364 nm. Therefore, the existence of the 420-nm band is confirmed by the resonance Raman profile which also enables its assignment as an

Table VI. C_{2v} Dimer Excited State Wave Functions and Energies

$$^1A_1 = {}^1/_2[|d_A\bar{\pi}^{nb}_\sigma| - |\bar{d}_A\pi^{nb}_\sigma| + |\pi^{nb}_\sigma\bar{d}_B| - |\bar{\pi}^{nb}_\sigma d_B|]$$

$$^1B_1 = {}^1/_2[|d_A\bar{\pi}^{nb}_\sigma| - |\bar{d}_A\pi^{nb}_\sigma| - |\pi^{nb}_\sigma\bar{d}_B| + |\bar{\pi}^{nb}_\sigma d_B|]$$

$$^3A_1 = {}^1/_2[|d_A\bar{\pi}^{nb}_\sigma| + |\bar{d}_A\pi^{nb}_\sigma| - |\pi^{nb}_\sigma\bar{d}_B| - |\bar{\pi}^{nb}_\sigma d_B|]$$

$$^3B_1 = {}^1/_2[|d_A\bar{\pi}^{nb}_\sigma| + |\bar{d}_A\pi^{nb}_\sigma| + |\pi^{nb}_\sigma\bar{d}_B| + |\bar{\pi}^{nb}_\sigma d_B|]$$

$$E(^1A_1) = K_{d\pi} + J_{d\pi} + I_{d\pi} + L_{d\pi}$$

$$E(^1B_1) = K_{d\pi} + J_{d\pi} - I_{d\pi} - L_{d\pi}$$

$$E(^3A_1) = K_{d\pi} - J_{d\pi} - I_{d\pi} + L_{d\pi}$$

$$E(^3B_1) = K_{d\pi} - J_{d\pi} + I_{d\pi} - L_{d\pi}$$

$$K_{d\pi} = \langle d_A(1)\pi^{nb}_\sigma(2)|H_{dimer}|d_A(1)\pi^{nb}_\sigma(2)\rangle$$

$$J_{d\pi} = \langle d_A(1)\pi^{nb}_\sigma(2)|H_{dimer}|d_A(2)\pi^{nb}_\sigma(1)\rangle$$

$$I_{d\pi} = \langle d_A(1)\pi^{nb}_\sigma(2)|H_{dimer}|\pi^{nb}_\sigma(1)d_B(2)\rangle$$

$$L_{d\pi} = \langle d_A(1)\pi^{nb}_\sigma(2)|H_{dimer}|\pi^{nb}_\sigma(2)d_B(1)\rangle$$

azide-to-copper(II) charge-transfer transition.

Discussion

The effects of forming a μ-1,3 azide bridge on the charge-transfer features in structurally defined complexes have now been determined and can be used to evaluate the TDVC model. The charge-transfer features of a terminally bound azide consist of a single intense ($\epsilon \sim 2000$ M^{-1} cm^{-1}) charge-transfer band ~ 9000–$10\,000$ cm^{-1} above the d–d transitions. Upon formation of the μ-1,3 dimer, the average energy of this transition increases by ~ 1000 cm^{-1} and splits into two components separated by 3600 cm^{-1}. The intensity ratio of the μ-1,3 azide features is approximately 2:1 with the most intense band lying at higher energy. This confirms the TDVC prediction of a single charge-transfer transition in the monomer splitting into two transitions in the dimer and allows assignment of the band at 365 nm as the more intense A_1 component and the band at 420 nm as the B_1 component of the Π^{nb}_σ charge-transfer transition. However, a quantitative comparison of the experimental and predicted A_1/B_1 intensity ratios and the $A_1 - B_1$ energy splittings reveals significant differences. Although, the TDVC model predicts an A_1/B_1 ratio of 8.6, experimentally, the B_1 component is ~ 4 times as intense as predicted. This deviation in the intensity ratio has been accounted for by vibronic coupling between the A_1 and B_1 transitions. The calculated energy splitting of the A_1 and B_1 components in a μ-1,3 dimer, based on the coupling of independent transition moments and the experimental absorbance intensity, is much smaller than the experimental value. This deviation may be accounted for considering the electronic contributions to this energy splitting in some detail.

Just as a copper dimer has singlet and triplet components of the ground state (for the C_{2v} μ-1,3 structure, these are the $^1A_1$ and $^3B_1$ which are split by >1100 cm^{-1} as measured in susceptibility studies[17b] of $[Cu_2(L\text{-Et})(N_3)][BF_4]_2$), excited states in the dimer have four components, which are the symmetric and antisymmetric combinations of singlets and triplets (where only the singlets are considered in the TDVC model). For the azide Π^{nb}_σ to Cu(II) $d_{x^2-y^2}$ transition in the C_{2v} dimer, the four excited states are the $^1A_1$, $^1B_1$, $^3A_1$, and $^3B_1$. Insight into the energy splitting between these states may be obtained by operating with the dimer Hamiltonian, H_{dimer}, on the coupled chromophore wave functions[44] of the excited states to obtain expressions for the energy of each dimer excited state relative to the monomer. The wave functions and energy expressions for each of the four dimer excited states are listed in Table VI, where d_A and d_B represent the $d_{x^2-y^2}$ orbital on copper A or B, and the bar over the orbitals denote β spin.

The expression for the energy correction for each dimer excited state is the sum of four matrix elements. $K_{d\pi}$ is the classic two electron Coulomb integral which also includes one-electron terms arising from small geometric distortions on forming the dimer.

(40) Spiro, T. G.; Stein, P. *Ann. Rev. Phys. Chem.* **1977**, *28*, 501–521.
(41) Archibald, T. W.; Sabin, J. R. *J. Chem. Phys.* **1971**, *55*, 1821–1829.
(42) Albrecht, A. C.; Hutley, M. C. *J. Chem. Phys.* **1971**, *55*, 4438–4443.
(43) Siebrand, W.; Zgierski, M. K. *Excited States* **1979**, *4*, 2–136.

(44) (a) Hansen, A. E.; Ballhausen, C. J. *Trans. Faraday Soc.* **1965**, *61*, 631–639. (b) Ross, P. K.; Allendorf, M. D.; Solomon, E. I. *J. Am. Chem. Soc.* **1989**, *111*, 4009–4021.
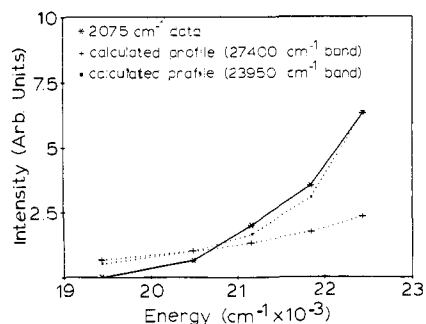
Spectroscopic Studies of Cu(II) Azide Complexes

J. Am. Chem. Soc., Vol. 111, No. 14, 1989 5207

Figure 14. Calculated resonance Raman A-term profiles for the asymmetric intraazide stretch in $[Cu_2(L\text{-}O\text{-})N_3][PF_6]_2$.
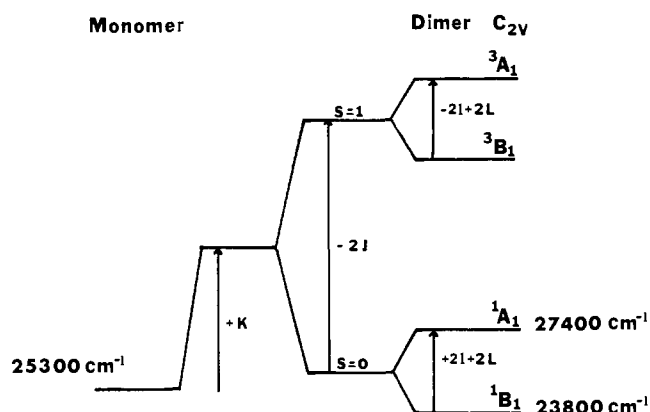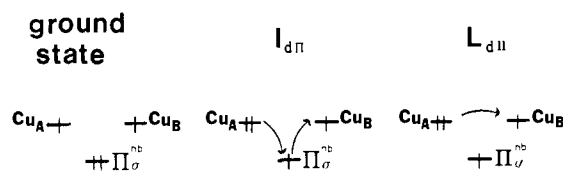

Figure 15. Energy splitting diagram of the four dimer excited states compared to the monomer energy levels. Experimentally observed energies (singlets) are included at right.

$K_{d\Pi}$ adds equally for all four of the dimer excited states and hence represents an average energy shift relative to the charge-transfer transition energy of the monomer (Figure 15). The second matrix element in the energy expression, $J_{d\Pi}$, is the excited state exchange integral, which causes the splitting of the singlet and triplet states in Figure 15. The terms $I_{d\Pi}$ and $L_{d\Pi}$ involve transfer of the charge-transfer excitation from Cu_A to Cu_B and produce the symmetric–antisymmetric splitting of the states. $I_{d\Pi}$ is the Coulomb-mediated excitation-transfer term and can be approximated by a multipole expansion. This is the energy splitting calculated in the TDVC model (eq 1). The $L_{d\Pi}$ matrix element in the energy expressions is the exchange-mediated excitation-transfer term (vide infra), which can also make a significant contribution to the symmetric–antisymmetric splitting.

As only the $^1A_1$ component of the dimer ground state is thermally populated, only the two singlet dimer states, $^1A_1$ and $^1B_1$, are spin and electric dipole allowed and thus experimentally observable. From Figure 15, it can be seen that the experimentally determined energies of the dimer $^1A_1$, $^1B_1$, and monomer transitions allow the experimental evaluation of the quantities $K_{d\Pi}$ + $J_{d\Pi}$ (the energy shift from monomer to dimer) and $2I_{d\Pi}$ + $2L_{d\Pi}$ (the splitting between $^1A_1$ and $^1B_1$). Recent studies on $Cu_2Cl_6{}^{2-}$ have found that a charge-transfer transition having good overlap with the ground-state orbital of the second copper exhibited a large antiferromagnetic excited state exchange interaction.[45] Thus, the large overlap of the azide $\Pi^{nb}{}_\sigma$ with the copper $d_{x^2-y^2}$ should lead to a large negative value of the excited state $J_{d\Pi}$. The experimental value of ~1000 cm^{-1} for $K_{d\Pi}$ + $J_{d\Pi}$ then requires a large positive value for $K_{d\Pi}$. The contribution of $I_{d\Pi}$ to the energy splitting of the $^1A_1$ to $^1B_1$ calculated by the TDVC model is 275 cm^{-1}, with the $^1A_1$ state to higher energy (Table V). The experimental splitting of 3600 cm^{-1} implies a value of 3325 cm^{-1} for $L_{d\Pi}$. This large value of $L_{d\Pi}$ is thus the origin of the deviation of the TDVC calculated splitting of the $\Pi^{nb}{}_\sigma$ to Cu $d_{x^2-y^2}$

(45) Desjardins, S. R.; Wilcox, D. E.; Musselman, R. L.; Solomon, E. I. *Inorg. Chem.* **1987**, *26*, 288–300.

Scheme II

Scheme III

charge-transfer state from the experimentally observed splitting.

Further insight into the origin of $L_{d\Pi}$ can be gained from the schematic representation of the interaction given in Scheme II. The excited state is formed by transfer of an electron from the $\Pi^{nb}{}_\sigma$ orbital on the azide to the $d_{x^2-y^2}$ orbital on Cu_A. $L_{d\Pi}$ then represents the transfer of this excitation to Cu_B through an exchange mechanism, where an electron moves from Cu_A to Cu_B. In comparison, $I_{d\Pi}$ represents the excitation transfer through a Coulomb mechanism, where an electron moves from Cu_A to the azide and a second electron moves from the azide to Cu_B. Thus, $I_{d\Pi}$ involves interacting dipoles, while $L_{d\Pi}$ proceeds through superexchange. The large positive experimental value of $L_{d\Pi}$ would seem to indicate that an excited superexchange pathway between the two coppers provides an efficient mechanism for excitation transfer. In oxy hemocyanin, the $^1A_1$ – $^1B_1$ splitting of the $\Pi^*{}_\sigma$ charge transfer has been found to be more than -4000 cm^{-1}.[6] As the TDVC calculated contribution for $I_{d\Pi}$ is -5000 cm^{-1}, the value of $L_{d\Pi}$ for oxy hemocyanin is less than 1000 cm^{-1}, significantly below the value for met azide hemocyanin. While the relative values of this splitting can be rationalized by qualitative estimates of the relative exchange pathways of the two exogenous bridging ligands, it is best approached by more quantitative molecular orbital calculations. Broken symmetry SCF-Xα-SW calculations of cis μ-1,2 peroxide and met azide sites are now in progress.

The information content of the vibrational data may be considered by examining Table II. When prepared with $^{14}N^{14}N^{15}N$, the asymmetric intraazide stretch splits into two components whose energy separation is dependent upon the coordination mode of the azide. Although the mixed isotope splitting correlates well with the geometric mode of azide binding, we have shown that it does not result from a simple mass effect of attaching copper(s) to one end of the azide but instead results from an inequivalence in bonding within the azide.[23] This inequivalence is reflected in the difference between the force constants $k(N1\text{-}N2)$ and k-$(N2\text{-}N3)$ which has been calculated for the series of complexes in Table II. A rationale for inequivalence within the bound azide is provided by considering the ground-state electronic structure of the coordinated azide in terms of contributions from the two resonance structures[46] in Scheme III. Prior work has attempted to relate the degree of asymmetry within the azide (i.e., the relative contribution of resonance structure B) to the magnitude of the asymmetric intraazide stretching frequency.[47] Exceptions to this generalization have been noted,[48] and an examination of Table II reveals that the asymmetric intraazide stretch is not diagnostic of the azide coordination mode. The N–N bond length [and corresponding $k(N\text{-}N)$] would also be expected to reflect this asymmetry. The resonance structures in Scheme III indicate that as the amount of single–triple character within the azide increases, the bond lengths should become more inequivalent, with N1–N2 > N2–N3. A Badger's rule relationship can be used to estimate the differences in bond lengths from the $k(N\text{-}N)$s.[49] This predicts

(46) Pauling, L. *The Nature of the Chemical Bond*; Cornell University Press: Ithaca, NY, 1967.

(47) Agrell, I. *Acta Chem. Scand.* **1971**, *25*, 2965–2974.

(48) Dori, Z.; Ziolo, R. F. *Chem. Rev.* **1973**, *73*, 247–254.

an inequivalence of ~0.01 Å for $[Cu_2(bpeac)(N_3)]^{2+}$, ca. 0.05–0.07 Å for a terminal azide, and ca. 0.10–0.12 Å for the μ-1,1 complexes.

Examination of Table II reveals several discrepancies between these predicted and the crystallographic bond lengths. In particular in both $[Cu_2(L'\text{-}O\text{-})(N_3)]$ and $[Cu_2(L\text{-}O\text{-})(N_3)]^{2+}$ the relative magnitudes of the N–N bond lengths are opposite to the ordering predicted by both the resonance structure model and the vibrational analysis. Furthermore, a correspondence of the magnitude of the calculated asymmetry is outside the crystallographic standard deviations for the appropriate N–N bond lengths.[16a,18] Several factors could be contributing to the observed lack of agreement. First, the crystal structures are exhibiting relatively large thermal parameters associated with the unbound nitrogens of the azide. The precision of the atomic positions of the azide nitrogens will also be affected by their close proximity to the heavier copper atoms. A small uncertainty in the position of the central azide nitrogen will have a large effect in the observed azide asymmetry. Finally, there is some disorder associated with the crystal structures as demonstrated by the relatively high R factors of 0.07–0.08. Thus for these systems the spectroscopy appears to be more sensitive than the crystallography to the nature of the intraazide bond.

The data in Table II indicate that the mixed isotope splitting of the asymmetric intraazide stretch is diagnostic of both the binding geometry of the azide and the inequivalence of the N–N bonds. Consideration of the calculated N–N force constants provides insight into differences in the bond order within the azide. A comparison of the N–N force constants from Table II with those calculated for an isolated single (F_2, 4.45 mdynes/Å), double (O_2, 11.39 dynes/Å), or triple bond (N_2, 22.41 mdynes/Å)[50] indicates that the N–N force constants in the μ-1,3 complexes are similar to those expected for a two double bond structure (resonance structure A). As the intraazide bonds become more inequivalent in the terminal and μ-1,1 structures, the bond orders acquire greater single–triple character. However, the largest inequivalence (the μ-1,1 complexes) still corresponds to approximately 60% resonance form A. In comparison to the μ-1,1 complexes, the 2150-cm^{-1} asymmetric intraazide stretch of HN_3 shows a similar 18 cm^{-1} $^{14,15}N_3$ isotopic splitting (2126.6 and 2144.6 cm^{-1})[51] which indicates that the inequivalence introduced by binding a proton or two copper(II)s to a single end of the azide are similar. The normal coordinate analysis of the HN_3 molcule also indicates that the two N–N force constants are similarly inequivalent (9.86 and 16.0 mdynes/Å).

The binding geometry of the azide in Busycon hemocyanin has been assigned as a μ-1,3 structure. As noted earlier, this was based on the observation of three azide-to-copper(II) charge-transfer bands and a 3.66 Å copper–copper distance. However, the 12 cm^{-1} mixed isotope splitting did not appear to be consistent with these results. An alternate explanation for the number of charge-transfer bands consistent with the mixed isotope data is the possibility of an azide terminally bound to each copper(II). The transition dipoles of the two terminal azides could then vector couple and produce four possible transitions. However, the data in Figure 10 require that a single azide binds to the site. Since the 3.66 Å copper–copper distance precludes a μ-1,1 geometry, the azide must bridge the two coppers in a μ-1,3 geometry. The apparent inconsistency between a μ-1,3 azide bridging geometry and the 12-cm^{-1} splitting of the asymmetric intraazide stretch can be rationalized by considering an additional interaction (such as hydrogen bonding) between the azide and a residue or water molecule in the protein pocket. If this interaction were localized at one end of the azide, it would tend to polarize the azide, creating an inequivalence between the nitrogen–nitrogen bonds which would account for the observed mixed isotope splitting.

The charge-transfer spectrum of met azide Busycon Hc can be interpreted by considering two limits for a μ-1,3 bridge: either the azide charge-transfer features result from two equivalent copper azide transition moments that couple (analogous to the μ-1,3 model complexes) or from two inequivalent transition moments, each providing a different charge-transfer band. These possibilities can be distinguished by the selection rules predicted for a C_{2v} dimer. From Table IV, the A_1 transition should be electric dipole allowed and thus observed in only the absorbance spectrum. The B_1 transition is both electric and magnetic dipole allowed and should contribute to both the absorbance and circular dichroism. Conversely, if the two coppers have inequivalent transition moments, C_1 symmetry is appropriate, and each transition would be expected to have both absorbance and CD intensity. The observed data for the hemocyanin (Figure 9) strongly indicates that the two copper azide transition moments are equivalent, since the higher energy absorbance feature at 370 nm has a larger absorbance intensity but little CD contribution, consistent with an A_1 assignment, while the B_1 band at 450 nm is relatively low in absorbance but has a large circular dichroism intensity.

A comparison of the energies and intensities of the charge-transfer features of met azide hemocyanin with those of the μ-1,3 model complexes further supports a μ-1,3 structure for met azide hemocyanin. Gaussian analysis of the met azide hemocyanin charge-transfer spectrum reveals the presence of two bands at 12 500 cm^{-1} (ϵ = 1900 M^{-1}) and 8100 cm^{-1} (ϵ = 900 M^{-1} cm^{-1}) above the ligand field transitions (Figure 9) which are similar to the charge-transfer energies and intensities observed for $[Cu_2(L\text{-}Et)(N_3)][BF_4]_2$ (Table I). However, it should be noted that the energy splitting of the Π^{nb}_σ transitions (4400 vs 3600 cm^{-1}) and the Gaussian resolved bandwidths (5500 vs 3750 cm^{-1}) are larger for the met azide hemocyanin as compared to the μ-1,3 model complex. Significant differences are observed between the resonance Raman profiles of met azide hemocyanin and $[Cu_2(L\text{-}Et)(N_3)][BF_4]_2$. While the profile of the asymmetric intraazide stretch in the μ-1,3 model complex peaks approximately 2000 cm^{-1} below the B_1 absorption peak maximum, the met azide hemocyanin excitation profile exhibits continually increasing intensity with increasing energy into the charge-transfer absorption band. It is difficult to compare the Raman profile of the weakly enhanced asymmetric copper azide stretch in $[Cu_2(L\text{-}Et)(N_3)][BF_4]_2$ with that of the asymmetric intraazide stretch due to the relatively poor signal to noise of the 358-cm^{-1} peak. However, in met azide hemocyanin, the resonance enhancement of the asymmetric copper azide stretch is larger, and its excitation profile peaks at 500 nm.

The asymmetric copper azide stretch in met azide hemocyanin could be exhibiting a B-term profile 2000 cm^{-1} lower than the B_1 charge-transfer band at 450 nm, similar to the observed profile of the asymmetric intraazide stretch in $[Cu_2(L\text{-}Et)(N_3)][BF_4]_2$. Alternatively, the increase in the intensity of the asymmetric copper azide stretch and its profile could indicate that an additional low-energy azide-to-copper(II) charge-transfer band is gaining intensity in the protein relative to the model complex. This alternative is supported by the presence of a 500-nm band in the absorbance spectrum of met azide Limulus (vide infra). A weak band at 500 nm must be a Π^{nb}_v transition. This increased intensity relative to the model complex may be accounted for by introducing a distortion of the μ-1,3 azide. Twisting the azide out of the plane of the two coppers would increase the overlap of the azide Π^{nb}_v and the copper $d_{x^2-y^2}$ orbitals allowing for increased intensity in the Π^{nb}_v transition. [The copper azide torsion angle is 7° in $[Cu_2(L\text{-}Et)(N_3)][BF_4]_2$.] Alternatively, an additional strong interaction with a residue in the protein pocket as indicated by the mixed isotope Raman data would also mix the Π^{nb}_σ and the Π^{nb}_v orbitals.

The differences in the azide charge-transfer spectra of the other coupled binuclear copper active sites in arthropod hemocyanin and tyrosinase may now be considered by extending this analysis of the Busycon (mollusc) met azide site. A comparison of the charge-transfer spectrum of Limulus (arthropod) Hc (Figure 16B) indicates qualitative similarity to that of Busycon Hc (Figure 16A),

(49) Badger, R. M. *J. Chem. Phys.* **1935**, *3*, 710–714.

(50) The force constants have been calculated from the following vibrational frequencies for O_2 (1554.7 cm^{-1}), N_2 (2330.7 cm^{-1}), and F_2 (892 cm^{-1}). Herzberg, G. *Molecular Spectra and Molecular Structure. I. Spectra of Diatomic Molecules*; Van Nostrand Reinhold: New York, NY, 1945; p 62.
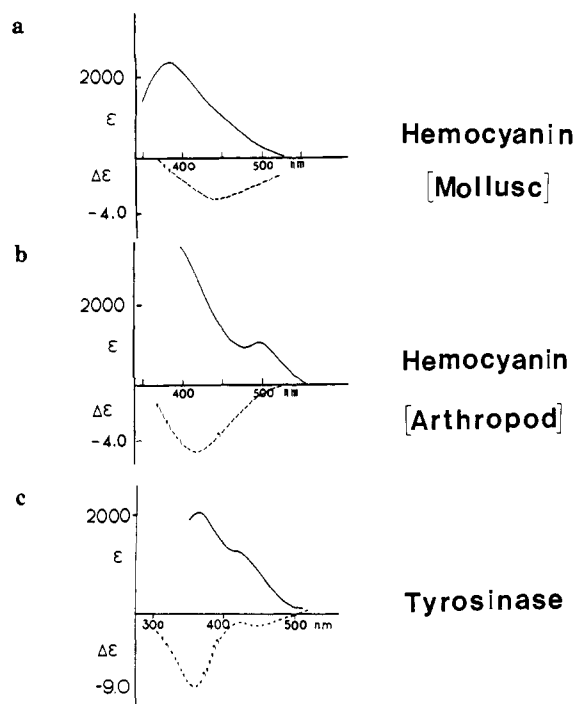
(51) Moore, C. B.; Rosengren, K. *J. Chem. Phys.* **1966**, *44*, 4108–4115.

Figure 16. Absorption (—) and circular dichroism (--) spectra of (top) met azide mollusc hemocyanin (Busycon); (middle) met azide arthropod hemocyanin (Limulus); (bottom) met azide tyrosinase (Neurospora).

showing analogous charge-transfer bands at 370 nm (ϵ = 2200 M^{-1} cm^{-1}) in absorbance and 420 nm ($\Delta\epsilon$ = -2 M^{-1} cm^{-1}) in the CD. However, the absorbance spectrum also exhibits an additional charge-transfer band at 500 nm (ϵ = 1000 M^{-1} cm^{-1}) which

corresponds to the peak in the Busycon resonance Raman profile. The CD absorbance selection rules observed in Busycon appear to hold for the Limulus site, indicating that the Limulus site can also be treated by considering two equivalent copper azide transition moments in a cis μ-1,3 structure. However, the 500-nm band is more intense in Limulus met azide which reflects a greater mixing of the Π^{nb}_σ and Π^{nb}_v orbitals and, thus, an increased distortion of the coordinated azide.

While the charge-transfer spectra of met azide tyrosinase (Figure 16C) show similar features in the absorbance spectrum (360 nm, ϵ = 2100 M^{-1} cm^{-1} and 420 nm, ϵ = 1400 M^{-1} cm^{-1}), the CD spectrum is quite different from that of the met azide hemocyanins. The intense 360-nm band has the dominant CD intensity ($\Delta\epsilon$ = -8.7 M^{-1} cm^{-1}), whereas the CD of the lower energy band is much weaker ($\Delta\epsilon$ = -2.1 M^{-1} cm^{-1}). Assuming one azide is binding, the presence of the two Π^{nb}_σ absorption bands at energies and intensities similar to the hemocyanins indicates that the azide also bridges the two copper(II)s. However, in contrast to the hemocyanins, the tyrosinase charge-transfer spectrum is more appropriately treated as resulting from two inequivalent copper azide transition moments because of the lack of the C_{2v} dimer absorbance-CD selection rules in Table IV. Thus, variations in the azide-to-copper charge-transfer spectra of the binuclear copper centers in the met arthropod and mollusc hemocyanins and tyrosinase appear to reflect quantitative structural differences in these coupled binuclear copper active sites and in particular inequivalent copper centers in the case of tyrosinase.

On the Mechanism of the Di-π-methane Rearrangement of Bicyclo[3.2.1]octa-2,6-diene: Deuterium Labeling and Generation of Diradical Intermediates via Photolysis and Thermolysis of Appropriate Azoalkanes

Waldemar Adam,*,[†] Ottorino De Lucchi,[‡] and Markus Dörr[1,†]

Contribution from the Institute of Organic Chemistry, University of Würzburg, Am Hubland, D-8700 Würzburg, F.R.G., and the Department of Organic Chemistry, University of Sassari, Via Vienna 2, I-07100 Sassari, Sardinia, Italy. Received July 13, 1988

Abstract: The direct (254 nm) and acetone-sensitized (300 nm) photolyses of 2,4,4-trideuteriobicyclo[3.2.1]octa-2,6-diene (D-1) gave exclusively 3,5,5-trideuteriotricyclo[4.2.0.0²,⁸]oct-3-ene (D-7) and 2,6,6-trideuteriotricyclo[3.2.1.0²,⁷]oct-3-ene (D-8) but no rearranged diene, namely, 2,8,8-trideuteriobicyclo[3.2.1]octa-2,6-diene (D-1'). Pyrolysis (400 °C) and direct (334 nm) and benzophenone-sensitized (364 nm) photolyses of the azoalkane 3,5,5-trideuterio-9,10-diazatricyclo[4.4.0.0²,⁸]deca-3,9-diene (D-9) afforded a mixture of tricyclooctenes D-7 (major product) and D-8 and bicyclooctadiene D-1, but no rearranged diene D-1'. These three modes of denitrogenation of the azoalkane 2,2,7-trideuterio-4,5-diazatricyclo[4.3.1.0³,⁷]deca-4,8-diene (D-10) led only to the tricyclooctene D-8 (major product) and equal amounts of the bicyclooctadienes D-1 and D-1'. Distinct temperature profiles were observed in the product fingerprints of the direct photolysis (334 nm) of the azoalkanes **9** and **10**. For both azoalkanes **9** and **10** the quantum yields of denitrogenation increased with rising temperature. In none of these transformations could bicyclo[3.3.0]octa-2,7-diene (**2**) be detected. These results imply that the di-π-methane rearrangement of the bicyclooctadienes **1** (D-1) and the denitrogenations of the azoalkanes **9** (D-9) and **10** (D-10) are disjoint chemical events. The intervention of diazenyl diradicals (one-bond cleavage of the azoalkanes) is postulated to be responsible for this disparity. The intervention of cyclopropyldicarbinyl diradical **3** as bona fide reaction intermediate in the di-π-methane rearrangement of bicyclooctadiene **1** is questioned.

In a recent publication[2] we demonstrated that the mechanism of the di-π-methane rearrangement of benzobicyclo[3.2.1]octa-

diene is more complex than initially proposed.[3] As suggested on the basis of deuterium labeling experiments for the related ben-

---

(1) Fonds der Chemischen Industrie Doctoral Fellow (1984-1986).